

Kondo Metal and Ferrimagnetic Insulator on the Triangular Kagomé Lattice

Yao-Hua Chen¹, Hong-Shuai Tao¹, Dao-Xin Yao^{2,*} and Wu-Ming Liu^{1†}

¹*Beijing National Laboratory for Condensed Matter Physics,
Institute of Physics, Chinese Academy of Sciences, Beijing 100190, China*

²*State Key Laboratory of Optoelectronic Materials and Technologies,
Sun Yat-sen University, Guangzhou 510275, China*

(Dated: May 24, 2018)

We obtain the rich phase diagrams in the Hubbard model on the triangular Kagomé lattice as a function of interaction, temperature and asymmetry, by combining the cellular dynamical mean-field theory with the continuous time quantum Monte Carlo method. The phase diagrams show the asymmetry separates the critical points in Mott transition of two sublattices on the triangular Kagomé lattice and produces two novel phases called plaquette insulator with an obvious gap and a gapless Kondo metal. When the Coulomb interaction is stronger than the critical value U_c , a short range paramagnetic insulating phase, which is a candidate for the short range resonating valence-bond spin liquid, emerges before the ferrimagnetic order is formed independent of asymmetry. Furthermore, we discuss how to measure these phases in future experiments.

PACS numbers: 71.30.+h, 75.10.-b, 05.30.Rt, 71.10.Fd

Geometrically frustrated systems have shown a lot of interesting phenomena, such as the spin liquid and spin ice [1–6]. The charge and magnetic order driven by interaction is still one of the central issues in the field of strongly correlation systems [7–12]. Recently, a new class of two-dimensional materials $Cu_9X_2(cpa)_6 \cdot xH_2O$ (cpa=2-carboxypentonic acid, a derivative of ascorbic acid; X=F, Cl, Br) has been found [13–15], which is formed by an extra set of triangles (B-sites in Fig. 1) insides of the Kagomé triangles (A-sites in Fig. 1). The Cu spins form a new type of geometrically frustrated lattice called triangular Kagomé lattice (TKL). This lattice can also be realized by cold atoms in the optical lattices, in which the interaction between trapped atoms can be tuned by Feshbach resonance and the kinetic energy can be adjusted by the lattice depth [16–22]. Although the effective spin models on this system have been investigated [7, 23], the real charge dynamics with spins and the phase diagram on this lattice have not been studied. Different with other frustrated system, such as the triangular lattice and Kagomé lattice, the “triangles-in-triangles” structure on the TKL induces two different sublattice. Therefore, it is desirable to investigate the Mott and magnetic transition on the TKL under the influence of asymmetry which is induced by different hoppings between two sublattices.

Recently, many analytical and numerical methods have been developed to investigate the strongly correlated system [24–31], such as the dynamical mean-field theory (DMFT) [32]. However, the DMFT works ineffectively in the frustrated systems because the nonlocal correlation and spatial fluctuations are ignored. Therefore, a new method called cellular dynamical mean-field theory (CDMFT) has been developed to incorporate spatially extended correlations and geometrical frustration in the framework of DMFT [33–36] by mapping the original lattice problem onto an effective cluster model coupled to an

effective medium. The continuous time quantum Monte Carlo method (CTQMC) [37] is employed as an impurity solver in the CDMFT loop, which is more accurate than the translational QMC method due to the absence of Trotter decomposition. So, the CDMFT combining with the CTQMC can provide useful numerous insights into the phase transitions in the frustrated system [8, 34].

In the present Letter, we employ the CDMFT combining with the CTQMC to investigate the influence of asymmetry on the Mott and magnetic phase transition on the TKL based on Hubbard model. Two novel phases called plaquette insulator and Kondo metal induced by asymmetry is found in the phase diagram and their properties is studied by determining the momentum resolved spectrums. By defining a magnetic order parameter, we can characterize a ferrimagnetic order for the large interaction on the TKL. The phase diagram with the competition between interaction and asymmetry is provided. In addition, the spectrum functions on the Fermi surface for the different interaction and asymmetry are presented. These interesting phases can be probed by the angle-resolved photoemission spectroscopy (ARPES) [38], neutron scattering, nuclear magnetic resonance (NMR) and other experiments.

We consider the standard Hubbard model on the TKL,

$$H = - \sum_{\langle ij \rangle \sigma} t_{ij} c_{i\sigma}^+ c_{j\sigma} + U \sum_i n_{i\uparrow} n_{i\downarrow} + \mu \sum_{i\sigma} n_{i\sigma}, \quad (1)$$

where t_{ij} is the nearest-neighbor hopping energy, U is the Coulomb interaction, μ is the chemical potential, $c_{i\sigma}^+$ and $c_{i\sigma}$ denote the creation and the annihilation operators, and $n_{i\sigma} = c_{i\sigma}^+ c_{i\sigma}$ corresponds to the density operator. The asymmetry factor is defined as $\lambda = t_{ab}/t_{bb}$, which can be adjusted by suppressing the samples in experiments. For the convenience, we use $t_{bb} = 1.0$ as the energy unit. As shown in Fig. 1(a), there are two different sublattices on the TKL called A-sites and B-sites. The

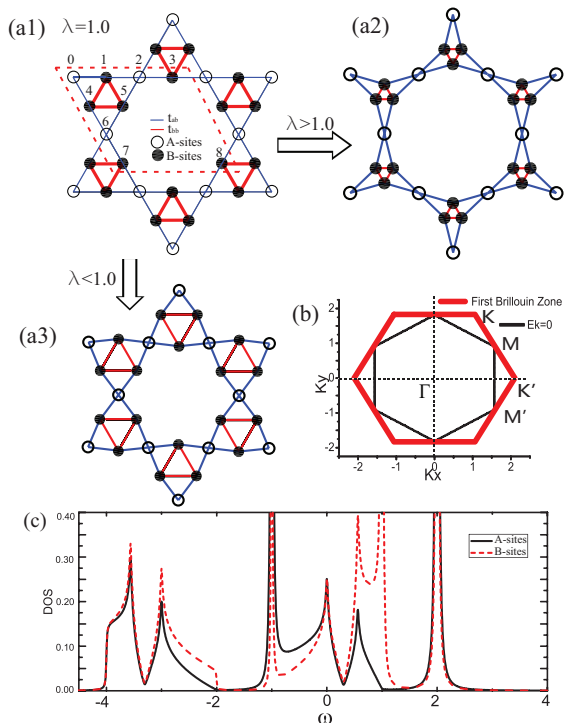


FIG. 1: (Color online) (a1) The unit cell of the triangular Kagomé lattice (TKL) without asymmetry ($\lambda = 1.0$). The open circles denote A-sites and the solid circles denote B-sites. The blue lines represent the hopping between A-sites and B-sites. And the red lines denote the hopping between B-sites. (a2) When $\lambda > 1.0$, the TKL is similar with the Kagomé lattice. (a3) When $\lambda < 1.0$, the TKL is transformed into a system composed of many triangular plaquettes. (b) The thick red lines show the first Brillouin zone of the triangular Kagomé lattice. The thin black lines correspond to the Fermi surface for the non-interacting case. The Γ, K, M, K', M' points denote the points in first Brillouin zone with different symmetry. (c) The density of states of the triangular Kagomé lattice for the A- and B-sites in the case of $U = 0$ and $\lambda = t_{ab}/t_{bb} = 1.0$.

space group of the TKL is $pm\bar{6}m$ same as the honeycomb lattice in the case of $\lambda = 1$, as show in Fig. 1(a1). Fig. 1(a2) shows the TKL is similar as the Kagomé lattice when $\lambda > 1$. We find the TKL can be transformed into a system composed of many triangular plaquettes in the case of $\lambda < 1$, as shown in Fig. 1(a3). The first Brillouin zone and Fermi surface of the symmetric TKL ($\lambda = 1$) with $U = 0$ is shown in Fig. 1(b). The density of states (DOS) for the different sublattices are shown in Fig. 1(c) in the case of $U = 0$ and $\lambda = 1$. They have the similar DOS around the Fermi surface.

We improve the CDMFT by combining it with the CTQMC to investigate the correlation effects on the TKL. In the CDMFT, the original lattice is mapped onto an effective cluster model via a standard DMFT procedure. Thus, the effective medium \hat{g} can be obtained by

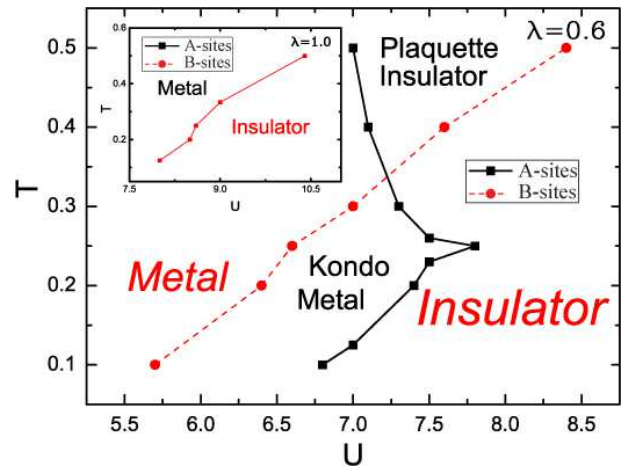


FIG. 2: (Color online) Phase diagram of the triangular Kagomé lattice at $\lambda = 0.6$ with $t_{bb} = 1.0$ as the unit of energy. The black solid lines with square points show the transition line of the A-sites, and the red dashed lines with circle points show the transition line of the B-sites. Two kinds of coexisting phases between red lines and black lines are the plaquette insulating phase and Kondo metal phase. Inset: The phase diagram of the symmetric TKL, i.e. $\lambda = 1$, in which there are no coexisting phases.

a Dyson equation:

$$\hat{g}^{-1}(i\omega) = \left(\sum_{\vec{k}} \frac{1}{i\omega + \mu - \hat{t}(\vec{k}) - \hat{\Sigma}(i\omega)} \right)^{-1} + \hat{\Sigma}(i\omega), \quad (2)$$

where $\hat{t}(\vec{k})$ is the hopping matrix element in the cluster, \vec{k} is the wave vector within the reduced Brillouin zone based on clusters, $\hat{\Sigma}(i\omega)$ is the self-energy matrix, and ω is the Matsubara frequency. Then, we introduce an impurity solver, such as the CTQMC, to calculate the cluster Green function $\hat{G}(i\omega)$. The new self-energy $\hat{\Sigma}(i\omega)$ can be calculated by Dyson equation $\hat{\Sigma}(i\omega) = \hat{g}^{-1}(i\omega) - \hat{G}^{-1}(i\omega)$ to close the self-consistent iterative loop. This CDMFT loop is repeated until the $\hat{\Sigma}(i\omega)$ converges to a desired accuracy. The CDMFT contains the important information of nonlocal correlation and geometrical frustration, which is absent in the general dynamical mean-field theory (DMFT). In addition, the absence of Trotter decomposition in the CTQMC makes this method more accurate than the translational auxiliary-field QMC.

The phase diagram obtained at $\lambda = 0.6$ shows two coexisting phases and a reentrant behavior of the Mott transition when half-filling. The asymmetry can cause the separation of the phase transition points of the A- and B-sites. As shown in Fig. 2, with an increasing interaction at $T = 0.5$, the A-sites are found to translate from a metallic phase into an insulating phase and the B-sites stay in the insulating phase. This phase is called the plaquette insulating phase shown in Fig. 2. In this plaquette insulating phase, electrons are localized on the A-sites and the absence of next nearest neighbor hop-

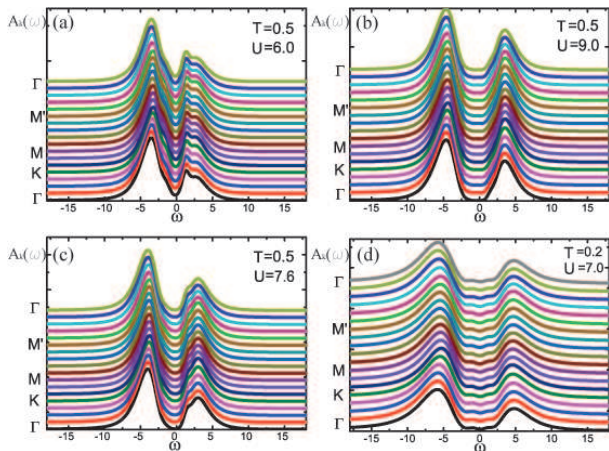


FIG. 3: (Color online) The momentum resolved one-particle spectrum $A_k(\omega)$ at $\lambda = 0.6$ in the units of $t_{bb} = 1$. (a) The metallic phase in the weak interaction case, such as $U = 6.0$ and $T = 0.5$. (b) The Mott insulating phase in the strong interaction case, such as $U = 9.0$ and $T = 0.5$. An obvious single particle gap shows up around the Fermi energy. (c) The plaquette insulating phase in the intermediate interaction case, in which the A-sites are insulating but B-sites are metallic, such as $U = 7.6$ and $T = 0.5$. A small gap shows up in this phase. (d) The Kondo metallic phase at $U = 7.0$ and $T = 0.2$, in which A-sites are metallic, B-sites are insulating. The single particle gap vanishes in this phase.

pings causes the electrons can only be itinerant within the B-sites. When $T < 0.34$, the B-sites translates into the insulating phase, however the A-sites remain in the metallic phase, see Fig. 2. This coexisting phase corresponds to a Kondo metal. The localized electrons on the B-sites act as the magnetic impurity, and the electrons on the A-sites are still highly itinerant. In this phase, the system shows the strong Kondo effect because of the high density of magnetic impurities. When the $U > U_c$, for example, $U_c = 7.6$ at $T = 0.25$, both the A-sites and B-sites translate into insulators. In Fig. 2, we find a reentrant behavior in the Mott transition of the A-sites caused by the frustration and the asymmetry, which is also found in the anisotropic triangular lattice [10]. This reentrant behavior divides the coexisting phases into two parts: the plaquette insulating phase and Kondo metallic phase. The inset figure in Fig. 2 shows the phase diagram of the TKL at $\lambda = 1.0$. There are no coexisting phase and reentrant behavior found on the TKL when the asymmetry is absent, i.e. $\lambda = 1$.

In order to find the properties of the different phases in Fig. 2, we investigate the momentum resolved one-particle spectrum $A_k(\omega)$ by using the Maximum Entropy Method (MEM) [39]. The results are shown in Fig. 3. The Γ, K, M and M' points have been defined in Fig. 1 (b). In the case of $T = 0.5$ and $U = 6.0$, we find two obvious quasi-particles near $\omega = 4.0$ and $\omega = 2.0$, see Fig. 3 (a). The gapless behavior shows that the system

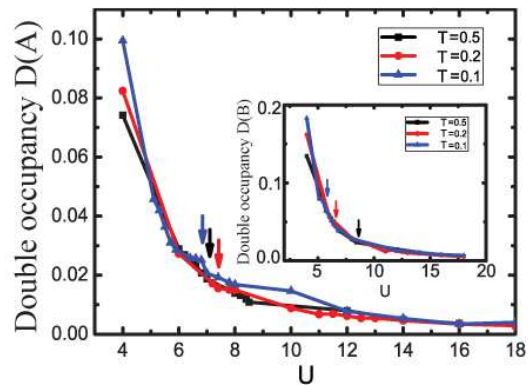


FIG. 4: (Color online) The evolution of double occupancy D on the A-sites as a function of interaction U with different temperatures at $\lambda = 0.6$ in the units of $t_{bb} = 1$. The inset figure shows the evolution of double occupancy on the B-sites. The arrows with different colors show the phase transition points at different temperatures.

stays in the metallic phase shown in Fig. 2. When the interaction U increases, we find an obvious gap near the Fermi energy (see Fig. 3 (b)), which indicates the system becomes an insulator denoted in Fig. 2. $A_k(\omega)$ of the plaquette insulating phase is shown in Fig. 3 (c). In Fig. 3 (d), we find there is no obvious gap near the Fermi energy when the system stays at the Kondo metal state in Fig. 2. The momentum resolved one-particle spectrum function can be obtained by the ARPES experiment, and the plaquette insulator and Kondo metal phases can be found in certain samples. We define the double occupancy D on the TKL as

$$D = \partial F / \partial U = \frac{1}{N} \sum_i \langle n_{i\uparrow} n_{i\downarrow} \rangle. \quad (3)$$

The decreasing of D on both sublattices shows that the suppressing of the itinerancy of electrons, which is a characteristic behavior of the Mott transition. When temperature drops, D increases due to the enhancing of the spin fluctuation at low temperature. The arrows indicate the phase transition point at different temperatures. The smoothly decreasing D characterizes a second order Mott transition when the interaction U increases.

In Fig. 5, we show the evolution of spectrum function on Fermi surface as a function of \vec{k} for different interactions U , temperature T and asymmetry λ , which is defined as

$$A(\mathbf{k}; \omega = 0) \approx - \lim_{\omega \rightarrow 0} \text{Im} G_k(\omega + i0) / \pi, \quad (4)$$

where

$$G_k(\omega) = \frac{1}{N} \sum_{\gamma, \delta} e^{i\mathbf{k} \cdot (\mathbf{r}_\gamma - \mathbf{r}_\delta)} [\omega + \mu - \hat{t}(\mathbf{k}) - \hat{\Sigma}(\omega)]_{\gamma\delta}^{-1}. \quad (5)$$

and k is the wave vector in the original Brillouin zone. A linear extrapolation of the first two Matsubara frequencies is used to estimate the self-energy to zero frequency

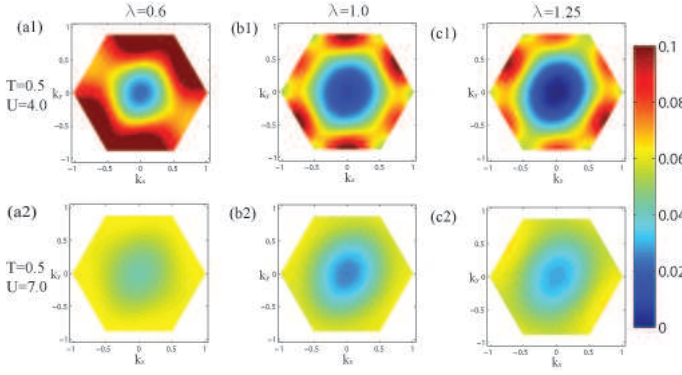


FIG. 5: (Color online) The evolution of the spectrum function on Fermi surface in the units of $t_{bb} = 1$. (a) $\lambda = 0.6$, (b) $\lambda = 1.0$, (c) $\lambda = 1.25$.

[36]. In the case of $\lambda = 1.0$, the spectrum function on Fermi surface shows six points near the M point in Fig. 1 (b), similar as the non-interacting case. When interaction U increases, the Fermi surface shrinks because of the localization of electrons. Fig. 5 (a1) shows the Fermi surface is similar as the system composed of many triangular plaquettes at $\lambda = 0.6$, due to the suppression of the hopping between the A-sites and the B-sites. The Fermi surfaces at $\lambda = 1.0$ and $\lambda = 1.25$ are similar as a Kagomé lattice. When the interaction U keeps increasing, the Fermi surface is developing into a flat plane showing the localization of electrons, see Fig. 5 (a2), (b2), and (c2). The spectrum function can be measured by the ARPES experiment.

In order to investigate the evolution of magnetic order on the TKL, we define a ferrimagnetic order parameter by:

$$m = \frac{1}{N} \sum_i \text{sign}(i) (\langle n_{i\uparrow} \rangle - \langle n_{i\downarrow} \rangle), \quad (6)$$

where $\text{sign}(i) = +1$, for $i=0, 2, 6$; and $\text{sign}(i) = -1$, for $i=1, 3, 4, 5, 7, 8$. Fig. 6 shows the evolution of the single particle gap ΔE and m as a function of interaction U in the case of $\lambda = 1.0$, $T = 0.2$. The Mott transition points of the A-sites and B-sites coexist when the asymmetry is absent. A gap opens in the case of $U = 8.5$. The ferrimagnetic order parameter $m = 0$ at $U < U_c = 13.8$ indicates the system is in a paramagnetic insulating phase. We argue that this paramagnetic insulating phase is a candidate for the short range RVB spin liquid due to the absence of long range correlations. When $U > U_c$, the finite m means the system enters a ferrimagnetic state. The inset picture of Fig. 6 shows the evolution of single particle gap ΔE at $\lambda = 0.6$ and $T = 0.5$, in which a gap opens on the A-sites first.

Finally, we provide a phase diagram about the asymmetry λ and interaction U at $T = 0.2$, see Fig. 7. As the asymmetry factor λ increases, a coexisting zone

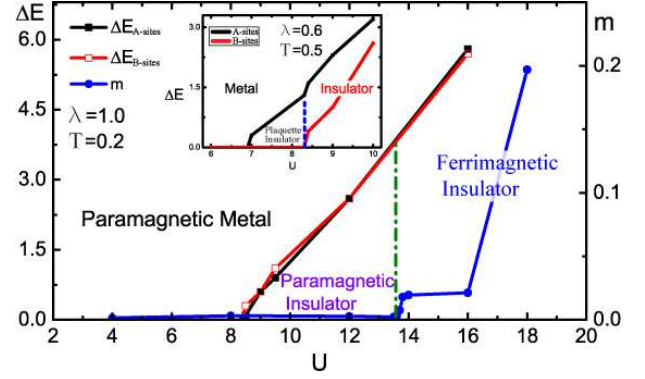


FIG. 6: (Color online) The evolution of single particle gap ΔE and ferrimagnetic order parameter m at $\lambda = 1.0$ and $T = 0.2$ in the units of $t_{bb} = 1.0$. A paramagnetic metallic phase is found when the interaction is weak with $\Delta E = 0$ and $m = 0$. As the interaction U increases, a gap is opened and no magnetic order is formed with $\Delta E \neq 0$ and $m = 0$. This paramagnetic insulating phase can be a short range RVB spin liquid. An obvious magnetic order is formed when the interaction is strong enough with $\Delta E \neq 0$ and $m \neq 0$. The insert picture shows the evolution of ΔE at $\lambda = 0.6$ and $T = 0.5$. A plaquette insulator is found when the A-sites are insulating and the B-sites are metallic.

containing the plaquette insulator and the Kondo metal shows up. This zone is suppressed from $\lambda = 0.9$ to $\lambda = 1.11$. When $U > U_c$, such as $U_c = 13.8$ in the case of $\lambda = 1.0$, the system becomes a ferrimagnetic insulator with $m \neq 0$. Before entering the ferrimagnetic phase, a paramagnetic insulator state is found. We argue this paramagnetic insulator state is a candidate of a short range RVB spin liquid due to the absence of any magnetic order and long range correlations.

In summary, we have obtained the rich phase diagrams as the function of interaction U , temperature T , and asymmetry factor λ . The asymmetry introduced in this strongly frustrated system can change the shape of the metal-insulator transition line and induces several interesting phases, such as plaquette insulator and Kondo metal. In the plaquette insulator phase, an obvious gap is found near the Fermi energy by investigating the momentum resolved spectrum function. The Kondo metal phase is an interesting phase where the partial sites work as the magnetic impurities in the metallic environment. We also find an interesting paramagnetic insulating phase which is related to the short range RVB spin liquid state before the ferrimagnetic order is formed. And the increasing of asymmetry does not suppress the emerging of this ferrimagnetic order. In addition, we have presented all kind of spectrum which can be used to detect these phases in real materials, such as $\text{Cu}_9\text{X}_2(\text{cpa})_6 \cdot x\text{H}_2\text{O}$, under applied pressure in experiments. Our studies provide a helpful step for understanding the coexisting behavior in metal-insulator transition, the formation of magnetic order and the emerging of spin liquid in frustrated systems

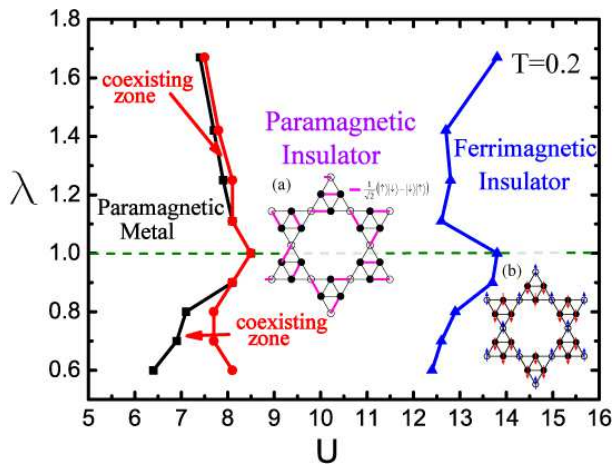


FIG. 7: (Color online) The phase diagram of the triangular Kagomé lattice represents the competition between interaction and asymmetry for $T = 0.2$ in the units of $t_{bb} = 1$. The region between the black lines with square points and the red lines with circle points denotes the coexisting zone which contains the plaquette insulator and the Kondo metal parts. A wide paramagnetic insulating region is found with an intermediate U . The blue lines with triangular points show the transition point to the ferrimagnetic insulator with a clear magnetic order. Insert: (a) Dimers formed in the paramagnetic insulator, which is a candidate for the short range RVB spin liquid, (b) Spin configuration of ferrimagnetic insulator.

with asymmetry.

We would like to thank N. H. Tong and S. Q. Shen for valuable discussions. This work was supported by the NKBRSCF under grants Nos. 2011CB921502, 2012CB821305, 2009CB930701, 2010CB922904, and NSFC under grants Nos. 10934010, 60978019, 11074310, and NSFC-RGC under grants Nos. 11061160490 and 1386-N-HKU748/10, and RFDPE of China (20110171110026).

* Electronic address: yaodaaox@mail.sysu.edu.cn

† Electronic address: wmliu@iphy.ac.cn

- [1] Z. Y. Meng et al., Nature (London) **464**, 847 (2010).
- [2] S. T. Bramwell et al., Nature (London) **461**, 956 (2009).
- [3] E. Mengotti et al., Nature Physics **7**, 68 (2011).
- [4] S. H. Lee et al., Nature Materials **6**, 853 (2007).
- [5] B. K. Clark, D. A. Abanin, and S. L. Sondhi, Phys. Rev. Lett. **107**, 087204 (2011).

- [6] M. Wang et al., Phys. Rev. B **84**, 094504 (2011).
- [7] Y. L. Loh et al., Phys. Rev. B **77**, 134402 (2008).
- [8] T. Yoshioka, A. Koga, and N. Kawakami, Phys. Rev. Lett. **103**, 036401 (2009).
- [9] Y. Kato et al., Nature Physics **4**, 614 (2008).
- [10] T. Ohashi, N. Kawakami, and H. Tsunetsugu, Phys. Rev. Lett. **97**, 066401 (2006).
- [11] M. Jarrell, and H. R. Krishnamurthy, Phys. Rev. B **63**, 125102 (2001).
- [12] W. Wu et al., Phys. Rev. B **82**, 245102 (2010).
- [13] M. Gonzalez, F. Cervantes-Lee, and L. W. ter Haar, Mol. Cryst. Liq. Cryst. Sci Technol. **233**, 317 (1993).
- [14] S. Maruti and L. W. ter Haar, J. Appl. Phys. **75**, 5949 (1993).
- [15] M. Mekata et al., J. Magn. Magn. Mater. **177**, 731 (1998).
- [16] D. Jaksch et al., Phys. Rev. Lett. **81**, 3108 (1998).
- [17] W. Hofstetter et al., Phys. Rev. Lett. **89**, 220407 (2002).
- [18] M. Greiner et al., Nature (London) **415**, 39 (2002).
- [19] L. M. Duan, E. Demler, and M. D. Lukin, Phys. Rev. Lett. **91**, 090402 (2003).
- [20] P. Soltan-Panahi et al., Nature Physics **7**, 434 (2011).
- [21] N. Gemelke et al., Nature (London) **460**, 995 (2009).
- [22] Y. H. Chen et al., Phys. Rev. A **82**, 043625 (2010).
- [23] A. Yamada et al., Phys. Rev. B **83**, 195127 (2011).
- [24] D. Galanakis, T. D. Stanescu, and P. Phillips, Phys. Rev. B **79**, 115116 (2009).
- [25] K. Aryanpour, W. E. Pickett, and R. T. Scalettar, Phys. Rev. B **74**, 085117 (2006).
- [26] C. C. Chang and S. W. Zhang, Phys. Rev. Lett. **104**, 116402 (2010).
- [27] W. Yao, and Q. Niu, Phys. Rev. Lett. **101**, 106401 (2008).
- [28] D. Xiao, W. Yao, and Q. Niu, Phys. Rev. Lett. **99**, 236809 (2007).
- [29] H. Lee, G. Li, and H. Monien, Phys. Rev. B **78**, 205117 (2008).
- [30] H. Terletska et al., Phys. Rev. Lett. **107**, 026401 (2011).
- [31] F. Zhou, Phys. Rev. Lett. **87**, 080401 (2001).
- [32] A. Georges et al., Rev. Mod. Phys. **68**, 13 (1996).
- [33] T. Maier et al., Rev. Mod. Phys. **77**, 1027 (2005).
- [34] H. Park, K. Haule, and G. Kotliar, Phys. Rev. Lett. **101**, 186403 (2008).
- [35] L. DeLeo, M. Civelli, and G. Kotliar, Phys. Rev. Lett. **101**, 256404 (2008).
- [36] O. Parcollet, G. Biroli, and G. Kotliar, Phys. Rev. Lett. **92**, 226402 (2004).
- [37] A. N. Rubtsov, V. V. Savkin, and A. I. Lichtenstein, Phys. Rev. B **72**, 035122 (2005).
- [38] A. Damascelli, Z. Hussain, and Z. X. Shen, Rev. Mod. Phys. **75**, 473 (2003).
- [39] M. Jarrell, and J. E. Gubernatis, Phys. Rep. **269**, 133 (1996).